INTERNATIONAL JOURNAL OF HYDROGEN ENERGY XXX (2017) 1–7

Available online at www.sciencedirect.com

ScienceDirect

journal homepage: www.elsevier.com/locate/he

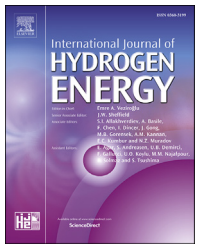

Research on a low temperature reversible solid oxide cell

Shaorong Wang [a,*], *Xing Hao* [b], *Weiting Zhan* [b]

[a] *School of Chemical Engineering and Technology, China University of Mining and Technology, 1st Da-xue Road, Xuzhou, Jiangsu 221116, China*

[b] *CAS Key Laboratory of Materials for Energy Conversion, Shanghai Institute of Ceramics, Chinese Academy of Sciences (SICCAS), 1295 Ding-xi Road, Shanghai 200050, China*

ARTICLE INFO

Article history:
Received 11 August 2017
Received in revised form
13 September 2017
Accepted 30 September 2017
Available online xxx

Keywords:
Infiltration
Stability
Low temperature reversible solid oxide cells

ABSTRACT

In this study, two-electrode-supported solid oxide cells with the structure of "Ni-Sm doped CeO_2 infiltrated porous $La_{0.9}Sr_{0.1}Ga_{0.8}Mg_{0.2}O_3$ (LSGM)| dense LSGM | $SmBa_{0.5}Sr_{0.5}Co_2O_5$ infiltrated porous LSGM" are fabricated. Fuel cell and steam electrolysis performance at different operating temperature (450–600 °C) for different steam content are tested, and reaction mechanism discussed. In the fuel-cell mode, the maximum power density reaches 1.817, 1.345, 0.801 and 0.342 W cm^{-2} at 600, 550, 500, and 450 °C, respectively. In electrolysis mode, current density at 1.3 V in 70% H_2O – 30% H_2 stream is −2.472, −1.616, and −0.727 A cm^{-2} at 600, 550, and 500 °C, respectively. The durability of the cell is tested for over 351 h.

Introduction

Reversible solid oxide cells (SOC) [1]can be operated in both electrolysis mode (SOEC: to store electricity energy with chemical fuels) and fuel-cell mode (SOFC: to convert fuels into electricity), which is considered as a promising energy storage technology [2–5]to balance the supply-demand mismatch for electricity from renewable energy such as solar and wind energy. Conventional SOFC using Yttria stabilized Zirconia (YSZ) as the electrolyte and Sr-doped $LaMnO_3$ (LSM) as the air electrode is called as high temperature SOFC, because the YSZ can only meet sufficient ionic conductivity, 0.1 S/cm, at around 1000 °C. So high an operating temperature severely limited the selection of component materials and hindered the commercialization of this technology [6].

Recently, there is a trend to reduce the operating temperature of SOCs into the so-called low temperature (LT) range (lower than 650 °C) for the following reason: at first, if the operating temperature could be decreased down to 500–600 °C, many waste heat sources in industry such as steel manufacturing or those from various combustors could be used for SOEC [7]; secondly, Fischer-Tropsch synthesis reaction [8,9] for directly synthesis of CH_4 [3] can be possible when stable electrolysis of CO_2 [10–12]can be realized on LT-SOCs; third, cheaper cost of components such as separators of SOC at low temperature would reduce the system cost [13]. For this purpose, however, the ohmic resistance and polarizations should be reduced by fine design of the cells and careful selection of materials.

* *Corresponding author.*
E-mail address: 5714@cumt.edu.cn (S. Wang).

https://doi.org/10.1016/j.ijhydene.2017.09.181

$La_{1-x}Sr_xGa_{1-y}Mg_yO_{3-0.5(x+y)}$ (LSGM) has sufficient ionic conductivity at reduced temperatures; it is stable and has no electronic conductivity in both oxidizing and reducing atmospheres. Because of such advantages, LSGM has been known as a very promising electrolyte material for intermediate temperature solid oxide fuel cells (IT-SOFC) [14–16] and solid oxide electrolysis cells (IT-SOEC) [17]. In contrast, Sm-doped ceria (SDC) or Gd-doped ceria (GDC) is not a good electrolyte for its partial reduction in reducing atmospheres, although it has comparable ionic conductivity as LSGM and is widely used as a barrier layer or a component in electrode materials [18]. In the temperature range lower than 650 °C, the thickness of LSGM film is expected to be reduced, and then electrode supported LSGM film, especially which supported from both sides, is the ideal choose. In this case, however, the thickness of electrodes increases from normal scale, and the risk of concentration polarization becomes the main concern; there are many model simulation works in the literature which reveal the importance of controlling the diffusion resistance [19–21].

Ni electrode has excellent activity and is a good catalyst for the H_2 formation during water splitting [22]. To avoid its reaction with LSGM and sintering at high manufacturing temperature, Ni is expected to be infiltrated into pre-sintered porous LSGM skeleton. The obtained nano-particles of Ni have high activity, but its sintering is the main reason of degradation. In our previous study, it has been confirmed that Ni-SDC infiltrated LSGM electrode is more stable and catalytically more active than Ni infiltrated LSGM electrode [23].

$SmBa_{0.5}Sr_{0.5}Co_2O_5$ is demonstrated a good cathode material, it has high conductivity and shows small area specific resistance (ASR) at intermediate temperatures [24]. And the recent studies show that infiltrated $SmBa_{0.5}Sr_{0.5}Co_2O_5$ has even higher catalytic activity and lower ASR [25].

Above materials have been widely studied in literature, but the assembly of them was mainly studied in the SOFC mode; the performance and its stability in SOEC mode is interesting but not well studied. In the present work, two-electrode-supported SOCs with the structure of "Ni-SDC infiltrated porous $La_{0.9}Sr_{0.1}Ga_{0.8}Mg_{0.2}O_3$ (LSGM)| dense LSGM | $SmBa_{0.5}Sr_{0.5}Co_2O_5$ infiltrated porous LSGM" are fabricated. The cells have the dense LSGM film as thin as 16 μm and are expected to have small ohmic resistance; infiltrated electrodes would also have low polarizations. The performance of the SOCs is tested and the stability discussed.

Experimental

Cell fabrications and characterization

The scaffold of the symmetrical cells with tri-layer structures of "porous LSGM | dense LSGM | porous LSGM" was fabricated by laminating one dense LSGM green tape and two porous LSGM green tapes on both sides with subsequent co-firing at 1380 °C for 4 h. The green tape for LSGM dense layer was prepared by tape casting technology. For this purpose, commercial LSGM powder was weighted and ball milled for 12 h, in the mixture of xylene and butyl acetate, with triethanolamine as dispersant. Then polyvinyl butyral (PVB) as binder, polyethylene glycol and dibutyl phthalate as plasticizer were added. The mixture was ball milled for 8 h to get the slurry, which was degassed in vacuum for 5 min, and tape casted on PET tape, following with drying at 50 °C, to get the green tape for the dense LSGM electrolyte film. As for the porous LSGM tape, similar procedure was adopted, but graphite as pole former was added to LSGM powder with the weight ratio being 1:5. During tape casting, the height of blade was 75 μm for the dense layer but 300 μm for the porous layer. During laminating of the green tapes, they were pressed under 3000 psi at 75 °C, and the hold time was 20 min. The green tri-layer tape of "porous LSGM | dense LSGM | porous LSGM" was cut to plates of 14 mm in diameter, and then sintered in air at 1380 °C for 4 h to get the LSGM skeleton of the symmetrical cells with ~20 μm thick dense LSGM electrolyte film in the middle.

For the preparation of $SmBa_{0.5}Sr_{0.5}Co_2O_5$(SBSC) electrode, solution for infiltration was prepared by weighting commercial $Sm(NO_3)_3\cdot 6H_2O$, $Ba(NO_3)_2$, $Sr(NO_3)_2$, $Co(NO_3)_2\cdot 6H_2O$ (all of them are AR grade in purity) and dissolving them into deionized water. Citric acid was added and its molar ration to the total metal ion was 1.2:1, the concentration of the solution was controlled to be around 0.5 mol L^{-1}. The solution was infiltrated into the porous LSGM layer, following by heat treatment at 500 °C for decomposition of the nitrates. This process was repeated several times until the final SBSC phase would be 20w% in the porous electrode. The previous work in our group shows that 21w% SBSC infiltrated LSGM skeleton gives the lowest polarization as a SOFC cathode [25]. The final heat treating temperature was selected as 900 °C (for 2 h), because samples treated independently at this temperature showed pure SBSC phase, while those treated at temperatures bellowing 850 °C showed XRD pattern of $SrCoO_3$ as impurity.

For the preparation of Ni-SDC electrode, similar procedure was adopted, but the start materials were $Sm(NO_3)_3\cdot 6H_2O$, $Ce(NO_3)_3\cdot 6H_2O$, and $Ni(NO_3)_2\cdot 6H_2O$ (also AR grade), the calculated Ni ratio in Ni/SDC mixture was 70w%, the weight ration of infiltrated active substance in the final electrode was controlled to be 20 w%, and the final treating temperature of the infiltrated Ni/SDC mixture was selected as 850 °C.

The morphologies of the cell configuration and infiltrated particles were characterized by scanning electron microscope (SEM, Hitachi S-4800-2).

Performance characterization

Initial performance of the cell was tested in both fuel-cell mode (FC mode) and electrolysis cell mode (EC mode). DC polarization (I–V) curves and Electrochemical impedance spectra (EIS) were measured at 450, 500, 550 and 600 °C, while a stream of H_2/H_2O mixture with different ratio (with the total flow rate being 100 sccm) was supplied to the Ni-SDC-LSGM hydrogen electrode and air supplied to the SBSC-LSGM oxygen electrode (flow rate 100 sccm).

Electrochemical impedance spectra (EIS) testing was performed using an IM6 Electrochemical Workstation (ZAHNER, Germany) between 10^5 and 10^{-1} Hz, with a 20 mV perturbation under open-circuits conditions. The ohmic resistance (R_o) was obtained from the value of the high frequency intercept. The electrode polarization resistances (R_p) were measured by the differences between the high and low frequency intersections of the impedance spectrum on the real axis (Z real axis).

Please cite this article in press as: Wang S, et al., Research on a low temperature reversible solid oxide cell, International Journal of Hydrogen Energy (2017), https://doi.org/10.1016/j.ijhydene.2017.09.181

Durability test

The durability of the cell was studied at 500 °C in both EC mode and FC mode, with 30% H_2–70% H_2O mixture for EC mode and 97% H_2–3% H_2O mixture for FC mode (total flow rate: 100 sccm) supplied to the Ni-SDC-LSGM hydrogen electrode and air supplied to the SBSC-LSGM oxygen electrode (flow rate 100 sccm). The cell was first operated at −0.6 A cm^{-2} (EC mode) for 206 h and then at 0.4 A cm^{-2} (FC mode) for 85 h and finally at −0.6 A cm^{-2} (EC mode) for 60 h.

Results and discussion

Fig. 1 (a) presents SEM image of the "porous LSGM| dense LSGM| porous LSGM" structure. The thickness of the porous LSGM layer and dense LSGM layer are 210 and 16 μm, respectively. Fig. 1 (b) and (b') show the SEM image of Ni-SDC-LSGM hydrogen electrode, while Fig. 1 (c) and (c') are for the SBSC-LSGM oxygen electrode, respectively. The micrograph shows that SBSC and Ni-SDC particles are evenly distributed on the surface of the LSGM skeleton with the particle size being 50–200 nm. Based upon mercury porosimetry measurements prior to catalyst infiltration, the porous LSGM layer has an overall porosity of 50% with pore size around 5 μm. After infiltration and reduction, the porosity of the Ni-SDC-LSGM electrode is estimated to be around 39%.

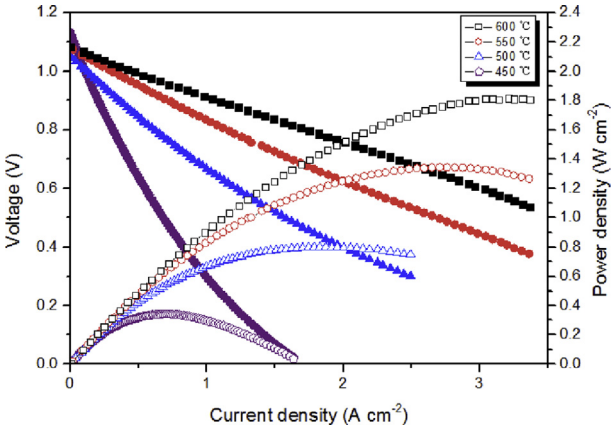

Fig. 2 – I–V curves and power densities in SOFC mode measured at 450–600 °C with 3% H_2O–97% H_2 as fuel and air as oxidant.

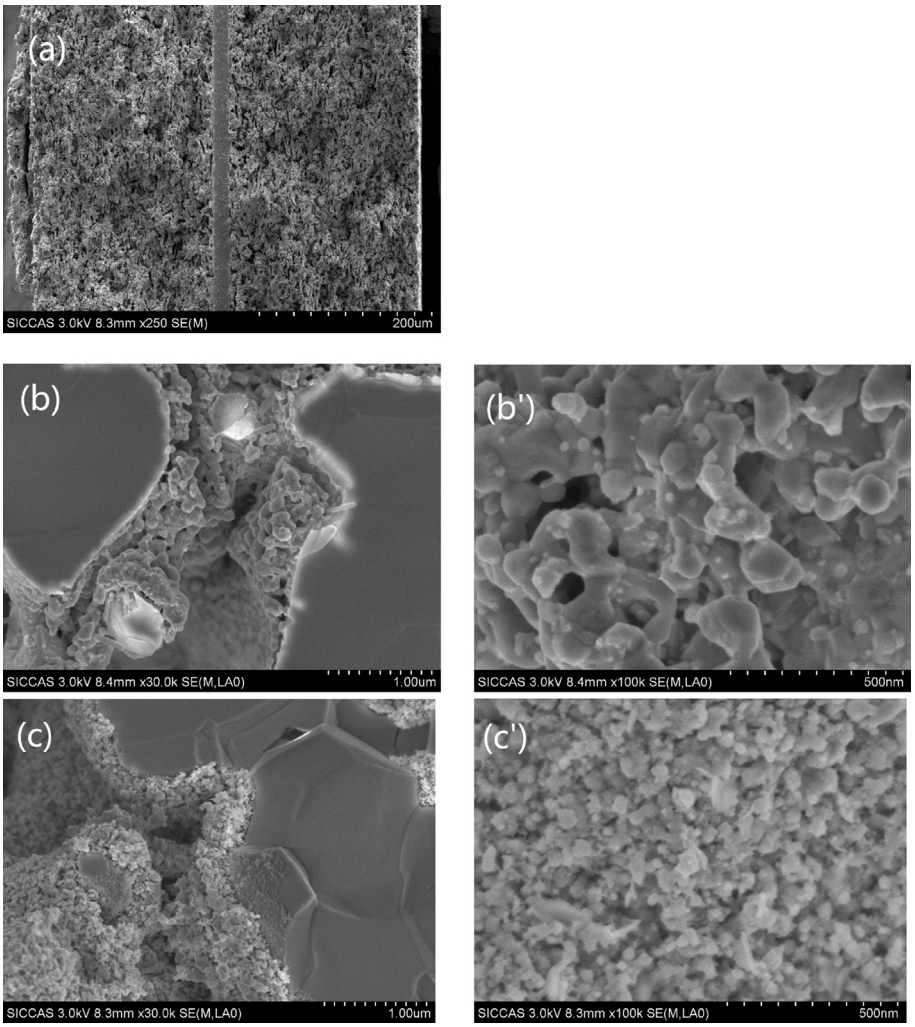

Fig. 1 – Cross-sectional SEM images of (a) cell configuration (b, b') Ni-SDC-LSGM hydrogen electrode (c, c') SBSC-LSGM oxygen electrode.

Please cite this article in press as: Wang S, et al., Research on a low temperature reversible solid oxide cell, International Journal of Hydrogen Energy (2017), https://doi.org/10.1016/j.ijhydene.2017.09.181

As is shown in Fig. 2, the maximum power density is 1.817, 1.345, 0.801 and 0.342 W cm^{-2} at 600, 550, 500, 450 °C, respectively.

As is shown in Fig. 3, the electrochemical impedance spectra of the SOCs above 500 °C are composed of two overlapping depressed arcs reflecting physical and/or chemical processes associated with the electrode reactions [26,27]. The EIS consist of two dominant arcs with summit frequencies of 10^2–10^3 Hz (mid-frequency) and 10^{-1}–10 Hz (low-frequency). The mid-frequency arcs, usually associated with the surface kinetics, decrease with the increase of temperature. At 450 °C, an obvious arc is observed at very high frequency, showing a different reaction mechanism. 450 °C may be too low and grain boundary resistance may become obvious.

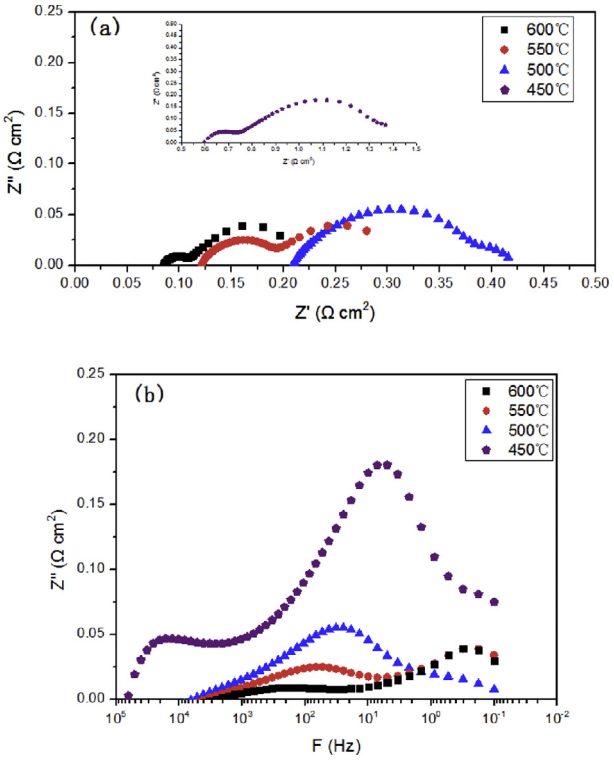

Fig. 3 – EIS measured at 450–600 °C with 3% H_2O–97% H_2 as fuel and air as oxidant at OCV: (a) Nyquist and (b) Bode plots.

The low-frequency arcs decreased with the temperature increasing from 450 to 500 °C and then increased with increasing temperature from 550 to 600 °C. The former is due to the increase of electrodes' activity, the latter, however, may have another reason. Since low frequency is attributed to gas phase diffusion, the increase of low-frequency arc can be explained by the insufficient supply of H_2O on the hydrogen electrode or O_2 on the oxygen electrode. The measurement was done at OCV with fixed 20 mV perturbation; the electrodes' activity and exchange current density will increase with increasing temperature. A larger exchange current density may cause more obvious diffusion polarization at low frequency. This may explain the abnormal increase of the low frequency arc above 500 °C.

Fig. 4 shows i-V curves for the SOC in H_2/H_2O mixtures at 500, 550, 600 °C. The gas mixtures used were 3% H_2O + 97% H_2, 50% H_2O + 50% H_2, and 70% H_2O + 30% H_2, respectively. Data are recorded for operation in both electrolysis mode (negative current) and fuel-cell mode (positive current).

As is shown in Fig. 4(a–c), the OCV decreases as the steam ratio increases, which can be predicted from the Nernst Equation for the hydrogen-oxygen-steam system.

$$E = E^{o} - \frac{RT}{nF} ln\left[\left(\frac{y_{H_2O}}{y_{H_2} y_{O_2}^{1/2}}\right)\left(\frac{p}{P_{std}}\right)^{-1/2}\right]$$

where E_0 is the Nernst potential at standard state, R is the gas constant (J mol^{-1} K^{-1}), T the temperature (K), n the number electrons transferred per molecule of steam electrolyzed, F the Faraday's constant (J V^{-1} mol^{-1}), P the test pressure (kPa), P_{std} the standard atmospheric pressure (kPa), and y_{H2}, y_{O2} and y_{H2O} are mole fractions of hydrogen, oxygen and water vapor, respectively.

For FC mode, the cell performance depends slightly on H_2O concentration, indicating the Ni-SDC infiltrated electrode possess sufficient stability and catalytic activity under high H_2O concentration.

As shown in the Fig. 4, the voltage data vary linearly with the current density up to a value (limiting current density) that depends on the temperature and the inlet H_2O concentration.

At 500 °C, as is shown in Fig. 4 (a), the i-V scan is fairly linear from 2 A cm^{-2} in the FC mode, through the OCV, to −2 A cm^{-2} in the EC mode in all H_2O concentrations. However, as temperature rises to 550 °C and 600 °C, shown in Fig. 4 (b) and (c), limiting current is observed in the SOEC mode for H_2O

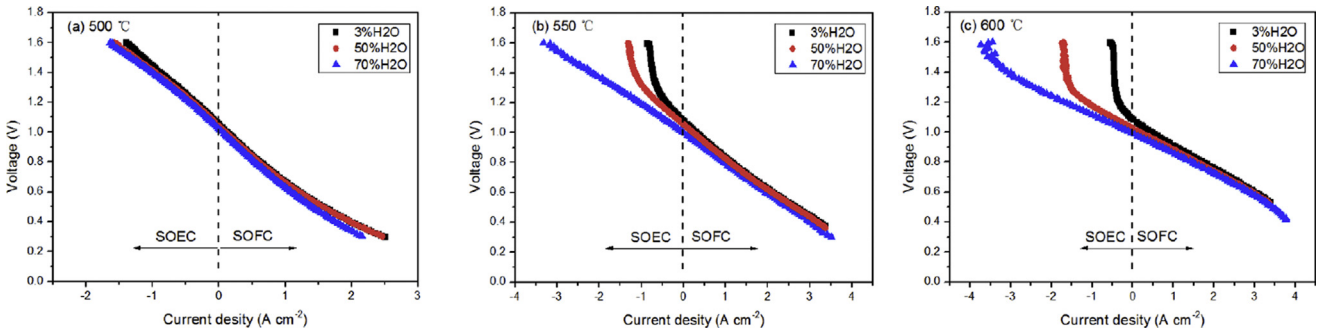

Fig. 4 – I–V curves measured with various H_2O concentrations in the fuel while air is flowing on the SBSC electrode: (a) 500 °C; (b) 550 °C; (c) 600 °C.

Please cite this article in press as: Wang S, et al., Research on a low temperature reversible solid oxide cell, International Journal of Hydrogen Energy (2017), https://doi.org/10.1016/j.ijhydene.2017.09.181

concentration of 3 and 50%, i.e. the I-V curves were approximately linear at low current density, but a rapid increase in cell voltage occurs at high current density. The limiting current densities increases for higher water concentrations, and then disappears as H_2O concentration rises to 70% at 550 °C but not fully disappears at 600 °C, which can be explained by the concentration polarization occurring at high current density, where H_2O diffusion becomes the rate limiting step.

Fig. 5 shows the Nyquist and Bode plots for different H_2O concentration at 500, 550 and 600 °C. The EIS consist of two dominant arcs with summit frequencies being 10^2–10^3 Hz (mid-frequency) and 10^{-1}-10 Hz (low-frequency). The mid-frequency arcs decrease with the increase of H_2O concentration and temperature, while the low-frequency arcs increase with the decrease of H_2O concentration and the increase of temperature. The mid-frequency arcs are significantly influenced by temperature but slightly by H_2O concentration. However, the low frequency arcs strongly depend on H_2O concentration. Since the mid-frequency arc is usually associated with the surface kinetics and low frequency is attributed to gas phase diffusion. EIS results confirmed that water diffusion becomes rate limiting as is also shown in Fig. 3 at high current density. Ro increases with increasing H_2O concentration at all the tested temperatures, which may be caused by the partial oxidation of Ni to NiO.

The durability of the cell was examined after the initial performance characterization. As shown in Fig. 6, reversible operation between electrolysis mode (−0.6 A cm^{-2}) and fuel cell mode (+0.4 A cm^{-2}) were performed. The current density of −0.6 A cm^{-2} gives a cell voltage close to the thermo-neutral voltage for steam electrolysis [3].

The cell voltage increased by about 45 mV (from 1.306 V to 1.351 V) during the first 206 h of electrolysis mode at −0.6 A cm^{-2}, which corresponds to a degradation of 1.7% 100 h^{-1}. During the next 85 h (from 206 h to 291 h) in fuel cell mode at 0.4 A cm^{-2}, a decrease in cell voltage of 69 mV (from

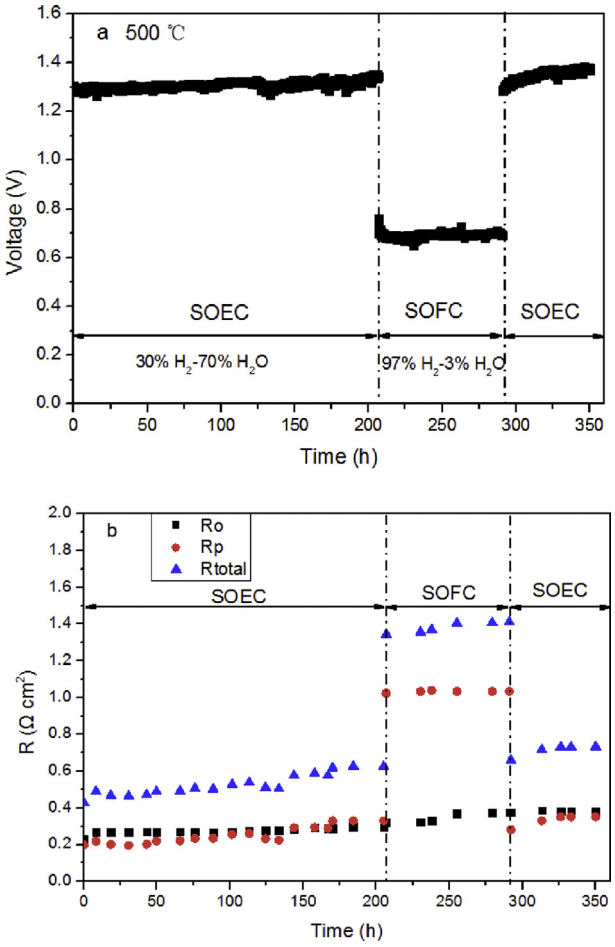

Fig. 6 – Variation of (a) Voltage vs time and (b) impedance components vs time.

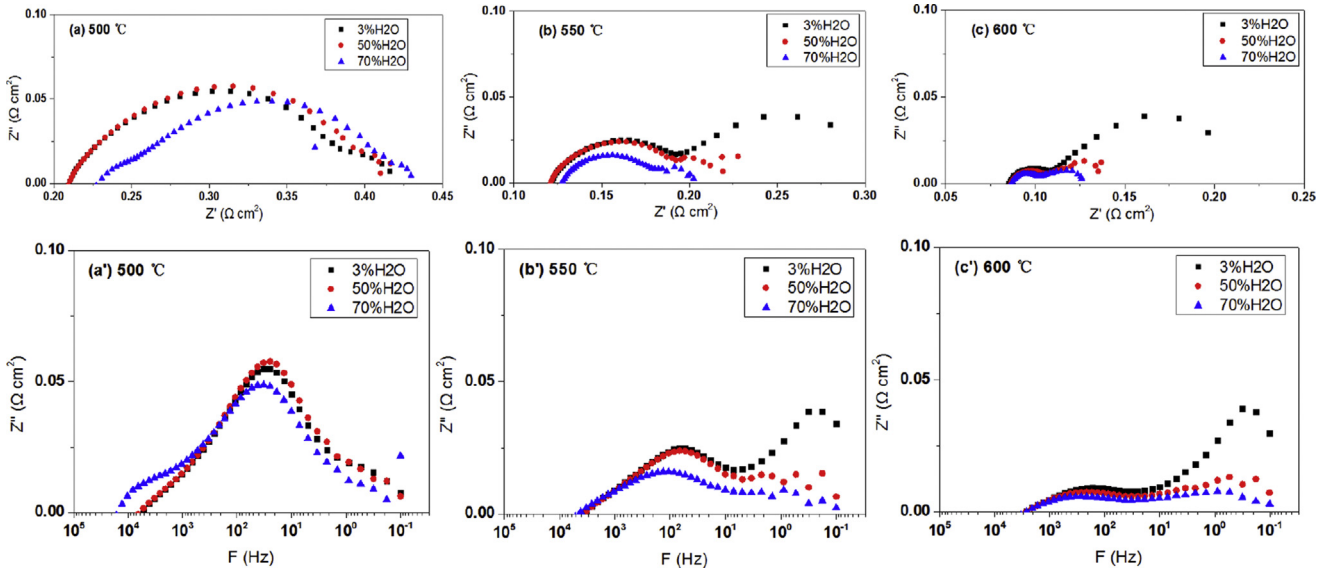

Fig. 5 – EIS measured under OCV at 450–600 °C with various H_2O concentration in the fuel: (a–c) Nyquist and (a'–c') Bode plots.

Please cite this article in press as: Wang S, et al., Research on a low temperature reversible solid oxide cell, International Journal of Hydrogen Energy (2017), https://doi.org/10.1016/j.ijhydene.2017.09.181

0.761 V to 0.692 V) or 10.7% 100 h^{-1} was observed. During the last stage of electrolysis mode over 60 h (from 291 h to 361 h) at −0.6 A cm^{-2}, the voltage increased 97 mV (from 1.282 V to 1.379 V), which corresponds to a degradation of 12.6% 100 h^{-1}.

Fig. 6 (b) shows the EIS measurements recorded throughout the galvanostatic tests at OCV. The R_o increased 0.066 Ω cm^{-2} (from 0.231 to 0.297 Ω cm^{-2}), 0.059 Ω cm^{-2} (from 0.319 to 0.378 Ω cm^{-2}), and −0.004 Ω cm^{-2} (from 0.386 to 0.382 Ω cm^{-2}), respectively for the three steps in the corresponding tested mode in Fig. 6 (a), with the corresponding degradation rate being 13.87%, 21.8% and −1.7% per 100 h, respectively. The whole R_o degradation rate was 18.6%.

The R_p increased for 0.131 Ω cm^{-2} (from 0.199 to 0.330 Ω cm^{-2}), 0.011 Ω cm^{-2} (from 1.024 to 1.035 Ω cm^{-2}), and 0.07 Ω cm^{-2} (from 0.282 to 0.352 Ω cm^{-2}), respectively, with the corresponding degradation rate being 31.9%, 1.2% and 41.3% per 100 h, respectively.

In order to understand the reason of degradation, we compared the SEM image of the electrodes before and after the durability test. As is shown in Fig. 7, the left pictures (a1, b1, c1, and d1) show the microstructure of electrodes before the test, while right pictures (a2, b2, c2, and d2) show those after the test. Obvious sintering phenomena are observed for both the hydrogen electrode and the oxygen electrode. Although the

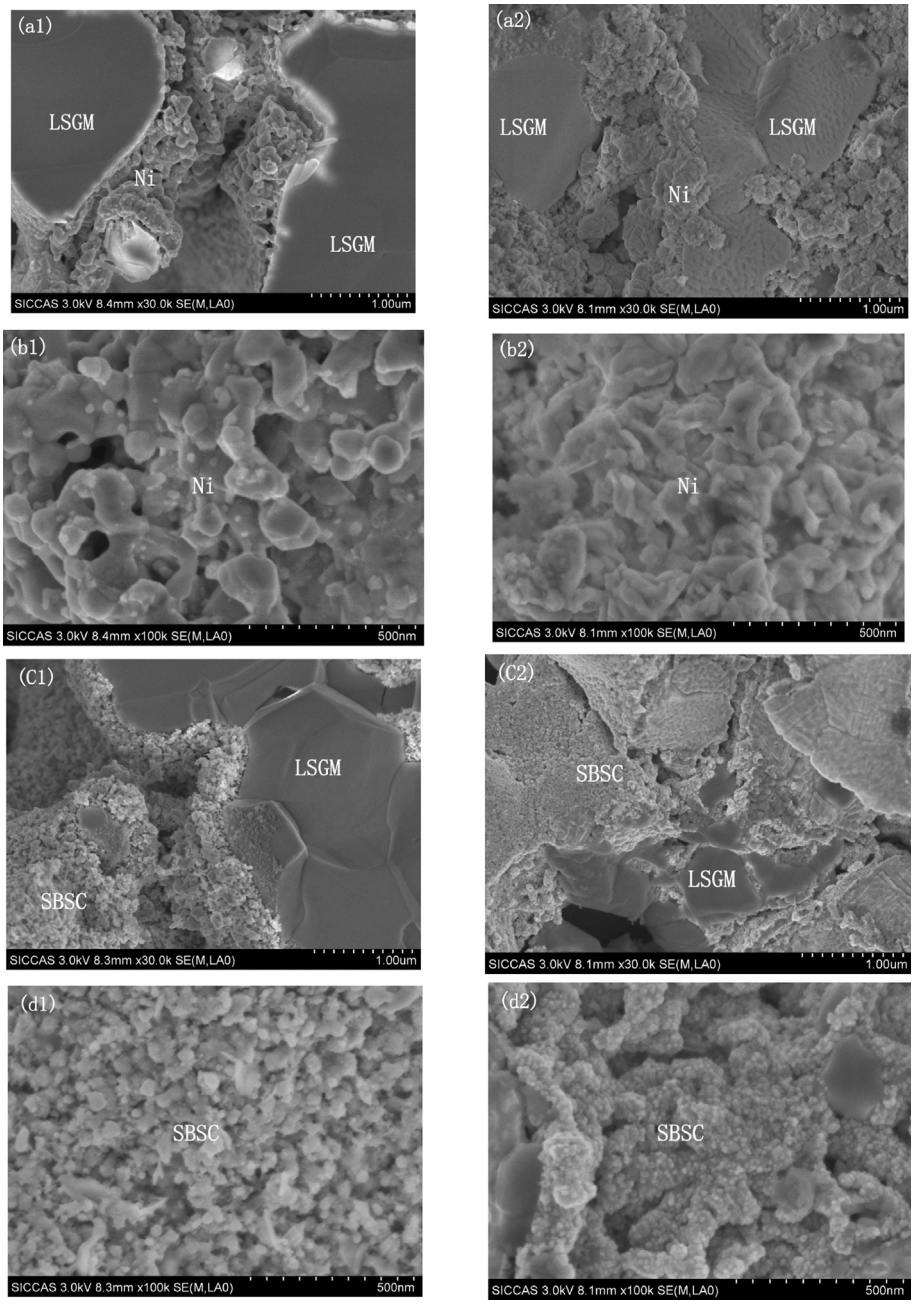

Fig. 7 – SEM images of the cell before and after the stability test: (a1)Ni-LSGM (b1)Ni particles (c1)SBSC-LSGM (d1)SBSC particles; (a2)Ni-LSGM (b2)Ni particles (c2)SBSC-LSGM(d2) SBSC particles.

Please cite this article in press as: Wang S, et al., Research on a low temperature reversible solid oxide cell, International Journal of Hydrogen Energy (2017), https://doi.org/10.1016/j.ijhydene.2017.09.181

active substances keep close contact to the LSGM skeleton, they form relatively dense layers to cover the LSGM particles. Densification of the active layers would reduce the triple phase boundary; some cracks also appear on the SBSC layer in picture c2. The structure change can explain the increase of both R_0 and R_p in Fig. 6. A nature material paper from Christopher Graves et al. reported that degradation of SOEC can be reduced by repeating shift operations between SOFC and SOEC mode, [2] and the result is observed for the cells of the type Ni–YSZ | YSZ | LSM–YSZ. But in our case, different result is obtained due to the difference in degradation mechanism.

For further work, it seems that main effort should be paid to prevent the sintering of the infiltrated particles, especially for SBSC.

Conclusions

We have developed two-electrode-supported LT-SOC with the structure "Ni-SDC infiltrated porous LSGM| dense LSGM | SBSC infiltrated porous LSGM". Excellent performance is shown for both SOFC and SOEC mode. However, a short-term test runs over 206 h in EC mode (-0.6 A cm^{-2}), 85 h in FC mode (0.4 A cm^{-2}) and then 60 h in EC mode (-0.6 A cm^{-2}) showed a quite fast degradation due to sintering of both Ni and SBSC particles.

Acknowledgment

We gratefully acknowledge the financial support from the National Basic Research Program of China (No. 2012CB215400), and National Natural Science Foundation of China (No. 51172266, No. 51302301, and No. 51672297). Mr. Xiaofeng Tong from SICCAS prepared the cells, his support is highly appreciated.

REFERENCES

[1] Mogensen M, Jensen SH, Hauch A, Chorkendorff I, Jacobsen T. Reversible solid oxide cells. In: Bansal NP, editor. Advances in solid oxide fuel cells III; 2008. p. 91–101.
[2] Graves C, Ebbesen SD, Jensen SH, Simonsen SB, Mogensen MB. Eliminating degradation in solid oxide electrochemical cells by reversible operation. Nat Mater 2015;14:239–44.
[3] Bierschenk DM, Wilson JR, Barnett SA. High efficiency electrical energy storage using a methane-oxygen solid oxide cell. Energy Environ Sci 2011;4(3):944–51.
[4] Xu NS, Li X, Zhao X, Goodenough JB, Huang K. A novel solid oxide redox flow battery for grid energy storage. Energy Environ Sci 2011;4(12):4942–6.
[5] Graves C, Ebbesen SD, Mogensen M, Lackner KS. Sustainable hydrocarbon fuels by recycling CO_2 and H_2O with renewable or nuclear energy. Renew Sustain Energy Rev 2011;15(1):1–23.
[6] Mahato N, Banerjee A, Gupta A, Omar S, Balani K. Progress in material selection for solid oxide fuel cell technology: a review. Prog Mater Sci 2015;72:141–337.
[7] Ishihara T, Jirathiwathanakul N, Zhong H. Intermediate temperature solid oxide electrolysis cell using $LaGaO_3$ based perovskite electrolyte. Energy Environ Sci 2010;3(5):665.
[8] Chen L, Chen F, Xia C. Direct synthesis of methane from CO_2-H_2O co-electrolysis in tubular solid oxide electrolysis cells. Energy Environ Sci 2014;7(12):4018–22.
[9] Becker WL, Braun RJ, Penev M, Melaina M. Production of fischer-tropsch liquid fuels from high temperature solid oxide co-electrolysis units. Energy 2012;47(1):99–115.
[10] Wang S, Ishihara T. Intermediate temperature CO_2 electrolysis by using $La_{0.9}Sr_{0.1}Ga_{0.8}Mg_{0.2}O_3$ oxide ion conductor. ISIJ Int 2015;55(2):381–6.
[11] Wang S, Tsuruta H, Asanuma M, Ishihara T. Ni-Fe-La(Sr) $Fe(Mn)O_3$ as a new active cermet cathode for intermediate-temperature CO_2 electrolysis using a $LaGaO_3$-Based electrolyte. Adv Energy Mater 2015;5(2).
[12] Shi Y, Luo Y, Cai N, Qian J, Wang SR, Li W, et al. Experimental characterization and modeling of the electrochemical reduction of CO_2 in solid oxide electrolysis cells. Electrochim Acta 2013;88:644–53.
[13] Wachsman ED, Lee KT. Lowering the temperature of solid oxide fuel cells. Science 2011;334(6058):935–9.
[14] Choy K, Bai W, Charojrochkul S, Steele BCH. The development of intermediate-temperature solid oxide fuel cells for the next millennium. J Power Sources 1998;71(1–2):361–9.
[15] Huijsmans JPP, van Berkel FPF, Christie GM. Intermediate temperature SOFC – a promise for the 21st century. J Power Sources 1998;71(1–2):107–10.
[16] Huang KQ, Tichy R, Goodenough JB. Superior perovskite oxide-ion conductor; strontium- and magnesium-doped $LaGaO_3$: III, performance tests of single ceramic fuel cells. J Am Ceram Soc 1998;81(10):2581–5.
[17] Ni M, Leung MKH, Leung DYC. Technological development of hydrogen production by solid oxide electrolyzer cell (SOEC). Int J Hydrogen Energy 2008;33(9):2337–54.
[18] Lawlor V. Review of the micro-tubular solid oxide fuel cell (part II: cell design issues and research activities). J Power Sources 2013;240:421–41.
[19] Udagawa J, Aguiar P, Brandon NP. Hydrogen production through steam electrolysis: model-based steady state performance of a cathode-supported intermediate temperature solid oxide electrolysis cell. J Power Sources 2007;166(1):127–36.
[20] Udagawa J, Aguiar P, Brandon NP. Hydrogen production through steam electrolysis: model-based dynamic behaviour of a cathode-supported intermediate temperature solid oxide electrolysis cell. J Power Sources 2008;180(1):46–55.
[21] Dumortier M, Lacroix O, Sanchez-Marcano J. Modeling of mass and energy transfers in a high temperature membrane electrolyser. Int J Hydrogen Energy 2014;39(9):4683–90.
[22] Aicart J, Petitjean M, Laurencin J, Tallobre L, Dessemond L. Accurate predictions of H_2O and CO_2 co-electrolysis outlet compositions in operation. Int J Hydrogen Energy 2015;40(8):3134–48.
[23] Han D, Liu Y, Wang SR, Zhan Z. Enhanced performance of solid oxide fuel cell fabricated by a replica technique combined with infiltrating process. Int J Hydrogen Energy 2014;39(25):13217–23.
[24] Kim JH, Cassidy M, Irvine JTS, Bae J. Electrochemical investigation of composite cathodes with $SmBa_{0.5}Sr_{0.5}Co_2O_{5+\delta}$ cathodes for intermediate temperature-operating solid oxide fuel cell. Chem Mater 2010;22(3):883–92.
[25] Han D, Wu H, Li J, Wang SR, Zhan Z. Nanostructuring of $SmBa_{0.5}Sr_{0.5}Co_2O_{5+\delta}$ cathodes for reduced-temperature solid oxide fuel cells. J Power Sources 2014;246:409–16.
[26] Huang Q-A, Hui R, Wang B, Zhan J. A review of AC impedance modeling and validation in SOFC diagnosis. Electrochim Acta 2007;52(28):8144–64.
[27] Nechache A, Cassir M, Ringuede A. Solid oxide electrolysis cell analysis by means of electrochemical impedance spectroscopy: a review. J Power Sources 2014;258:164–81.

Please cite this article in press as: Wang S, et al., Research on a low temperature reversible solid oxide cell, International Journal of Hydrogen Energy (2017), https://doi.org/10.1016/j.ijhydene.2017.09.181